CHEMISTRY OF MATERIALS

ARTICLE

pubs.acs.org/cm

Evaluation of Homoleptic Guanidinate and Amidinate Complexes of Gadolinium and Dysprosium for MOCVD of Rare-Earth Nitride Thin Films

Tobias B. Thiede,[†] Michael Krasnopolski,[†] Andrian P. Milanov,[†] Teresa de los Arcos,[‡] Andreas Ney,[§] Hans-Werner Becker,[⊥] Detlef Rogalla,[⊥] Jörg Winter,[‡] Anjana Devi,*[,†] and Roland A. Fischer*[,†]

[†]Inorganic Chemistry II, Ruhr-University Bochum, 44801 Bochum, Germany

[‡]Experimental Physics II, Ruhr-University Bochum, 44801 Bochum, Germany

[§]Fachbereich Physik and CENIDE, Universität Duisburg-Essen, Lotharstr 1, D-47057 Duisburg, Germany

[⊥]Dynamitron-Tandem-Laboratorium (DTL) of RUBION, Ruhr-University Bochum, 44801 Bochum, Germany

Supporting Information

ABSTRACT: Metal−organic chemical vapor deposition (MOCVD) of thin films of two representative rare-earth nitrides is reported here for the first time. Four homoleptic, all-nitrogen-coordinated, rare-earth (RE) complexes were evaluated as precursors for the respective nitride thin film materials. Two guanidinato complexes $[RE\{(^{i}PrN)_2C(NMe_2)\}_3]$ [RE = Gd (**1**), Dy (**2**)] and two amidinato complexes $[RE\{(^{i}PrN)_2CMe\}_3]$ [RE = Gd (**3**), Dy (**4**)] were compared and used either as single source precursors or together with ammonia for MOCVD of gadolinium nitride (GdN) and dysprosium nitride (DyN), respectively. The thermal properties of the precursors were studied and the fragmentation patterns were characterized by high-resolution electron impact−mass spectrometry (HR EI-MS). The obtained nitride films were investigated using a series of techniques, including X-ray diffraction (XRD), scanning electron microscopy (SEM), nuclear reaction analysis (NRA), Rutherford backscattering (RBS), and X-ray photoelectron spectroscopy (XPS). The films contain preferentially oriented grains of fcc-GdN and DyN and are contaminated with small amounts of carbon and oxygen (significantly below 10 at. % in the best cases).

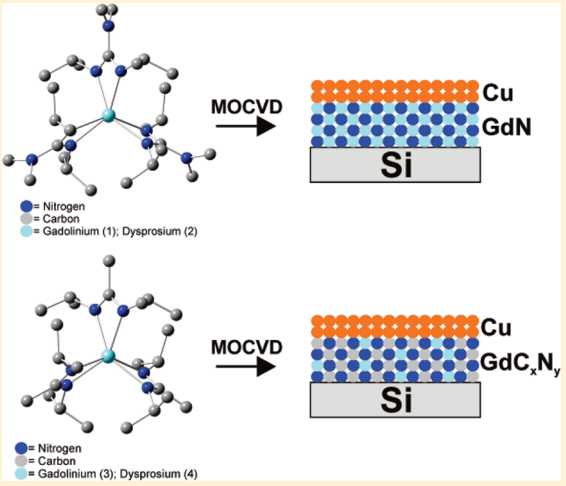

The temperature-dependent magnetic properties of the films, as measured using a superconducting quantum interference device (SQUID), suggest the existence of small ferromagnetic grains of the rare-earth nitrides that exhibit superparamagnetism. Despite the chemical and structural similarity of the guanidinato and amidinato complexes (**1**−**4**), a distinctly different behavior as MOCVD precursors was found for **1** and **2**, compared with that for **3** and **4**. While the guanidinates operate well as single-source precursors (SSPs), the amidinates are not suited at all as SSPs, but give very good nitride films when used in the presence of ammonia. This characteristic behavior was correlated with the different fragmentation mechanisms, as revealed by EI-MS.

KEYWORDS: chemical vapor deposition, magnetic materials

INTRODUCTION

Rare-earth (RE) nitride materials possess unique magnetic, electronic, and optical properties, which makes them very interesting for a number of applications.[1,2] For example, gadolinium nitride (GdN) is a promising material for spintronics and it has been investigated recently from theoretical and experimental points of view.[3,4] Also, dysprosium nitride (DyN) was investigated as a material for ferromagnet/semiconductor superlattice structures,[5] which might be of importance for spintronic applications as well. The syntheses of bulk rare-earth nitrides using $[RE\{N(SiMe_3)_2\}_3]$ in the presence of ammonia or reacting rare-earth chlorides with lithium nitride have been reported.[6,7] However, only limited data on the preparation or deposition of RE nitride thin films and their properties exist in the literature, which is partly due to the difficulty of handling this class of materials. The high oxophilicity of RE nitrides, their high reactivity toward air, as well as the high melting point of RE metals, call for sophisticated experimental techniques to fabricate pure RE nitride thin films. Physical vapor deposition (PVD) techniques, such as molecular beam epitaxy (MBE),[8] ion-assisted deposition (IAD),[9] and Ar/N_2 mixed-gas-plasma radio frequency (rf) sputtering[10] were used to physically deposit GdN thin films under UHV conditions. Recently, we reported on the first chemical preparation of GdN thin films by means of metal−

Received: October 1, 2010
Revised: December 8, 2010
Published: February 24, 2011

organic chemical vapor deposition (MOCVD).[11] In contrast to simple physical deposition, which usually shows poor step coverage and low throughput, chemical deposition methods (in particular, MOCVD and the related atomic layer deposition (ALD)) is generally more suitable for industrial applications, because of large area deposition with uniform and conformal coverage. However, MOCVD and ALD techniques heavily depend on the underlying precursor chemistry and can only be successfully employed if the precursor chemistry in general and the basic steps of the chemical deposition process in particular are well-understood.[12] Therefore, metal−organic precursors with tailored properties need to be developed via variation of the ancillary ligand system, and these precursors and processes need to be optimized individually.[13] This is especially true for metal nitride precursors.[14] It was shown that amido and imido ligands are useful for the synthesis of transition-metal complexes, which can act as precursors for transition-metal nitrides.[15−22] More recently, all-nitrogen-coordinated, heteroleptic derivatives of the simple amido/imido-compounds containing chelating monoanionic guanidinato ligands, $\{(R'N)_2C(NR''_2)\}^-$ (R′, R″ = alkyl substituents, such as Me, Et, ^{i}Pr), in the coordination sphere of Ta, Nb, Mo, and W were investigated, and, in some cases, superior performance as precursors for the nitrides was reported.[23,24] We successfully transferred these precursor concepts to the family of homoleptic guanidinato precursors of lanthanide metals with GdN as a representative test case. $[Gd\{(^iPrN)_2C(NMe_2)\}_3]$ (**1**) turned out to be a surprisingly good single-source precursor for the growth of phase-pure, rock salt GdN by MOCVD, and similar behavior was indicated for the dysprosium analogue $[Dy\{(^iPrN)_2C(NMe_2)\}_3]$ (**2**).[11,25] Employing high-resolution electron impact mass spectrometry (HR EI-MS), the Gd-imido species were detected in the course of the fragmentation of **1**, supporting the idea that the guanidinato ligand serves as a source for the N component under single-source MOCVD conditions.[26,27]

Amidinate ligands, $\{(R'N)_2CR''\}^-$, are quite similar to guanidinates, $\{(R'N)_2C(NR''_2)\}^-$, differing only by exchange of NR''_2 by R′, and they have been recognized as being very good ligands of precursors for ALD of RE metal oxide thin films.[28−31] To further explore the pluripotent potential of such precursors we set out to compare the closely related homoleptic guanidinates $[RE\{(^iPrN)_2CNMe_2\}_3]$ (**1**, RE = Gd; **2**, RE = Dy) with the amidinates $[RE\{(^iPrN)_2CMe\}_3]$ (**3**, RE = Gd; **4**, RE = Dy), which are all-nitrogen-coordinated complexes, as precursors for MOCVD of the respective rare-earth nitride (REN) materials. The chemical and thermal properties of **1**−**4** were thoroughly investigated by routine EI-MS, high-resolution EI-MS, thermogravimetric (TG) analysis, and isothermal TG studies. Interestingly, no rare-earth imido fragments were detected during EI fragmentation of the amidinates **3** and **4**. Instead, metal alkyl fragments were identified by high-resolution mass spectrometry (HR EI-MS). The different fragmentation property turned out to correlate with a quite different behavior in the MOCVD experiments, either performed under single-source conditions or together with ammonia as an additional source of nitrogen. The deposited REN films were characterized ex situ by X-ray diffraction (XRD) and scanning electron microscopy (SEM) to analyze the thickness and morphology of the films. Nuclear reaction analysis (NRA) was performed to investigate the ratio between the light elements (C, N, and O) within the bulk of the films. Rutherford backscattering analysis (RBS) and X-ray photoelectron spectroscopy (XPS) were performed to investigate the ratio of the light elements and the metal inside the films. Depth profiles of the elemental composition of the films were achieved employing XPS. Magnetic measurements were done on selected films using a SQUID device. Note, that prior to these ex situ analyses, a protective layer of copper was deposited atop the REN films in a subsequent MOCVD process, to slow the oxidation of the films (post-deposition).[9] Copper was selected since it was easy to deposit in situ with our MOCVD screening apparatus.

EXPERIMENTAL SECTION

Precursor Synthesis. The complexes *tris*(*N*,*N*′-diisopropyl-2-dimethylamido-guanidinato)-gadolinium(III) $[Gd(DPDMG)_3]$ (**1**) and *tris*(*N*,*N*′-diisopropyl-2-dimethylamido-guanidinato)-dysprosium(III) $[Dy(DPDMG)_3]$ (**2**) were synthesized following the procedure published earlier.[25] The complexes *tris*(*N*,*N*′-diisopropyl-acetamidinato)-gadolinium(III) $[Gd(DPAMD)_3]$ (**3**) and *tris*(*N*,*N*′-diisopropyl-acetamidinato)-dysprosium(III) $[Dy(DPAMD)_3]$ (**4**) were synthesized following a similar procedure as reported for the guanidinato complexes.[25] *Bis*(1-dimethylamino-2-propanolato)copper(II) $[Cu(dmap)_2]$ (**5**) was synthesized following the procedure published by Buhro et al.[32] All reactions were performed using a conventional vacuum/argon line and standard Schlenk techniques. The precursors were purified by sublimation in vacuum (125 °C, 5×10^{-2} mbar dynamic vacuum). The purity of the precursors was confirmed using high-resolution EI-MS, ^{1}H NMR, and elemental analysis. High-resolution electronic ionization mass spectra (HR EI-MS) were recorded, using a Varian MAT spectrometer. NMR was recorded on a Bruker Advance DPX 250 spectrometer and elemental analysis data were obtained on a CHNSO Vario EL analyzer, respectively. The preparation of samples for analysis was carried out in an argon-filled glovebox (MBraun). Thermogravimetric analysis (TGA) data were obtained on a Seiko Model TG/DTA 6300S11 instrument. The measurements were performed under inert gas atmosphere at ambient pressure. Approximately 10 mg of each sample were filled in aluminum crucibles with a circular opening (diameter of 5 mm). The heating rate was 5 °C/min, and a nitrogen flow of 300 mL/min was used. The thermal behavior of **3** and **4** was further investigated by isothermal TGA studies. For each study, the sample was held at a fixed temperature (80 or 125 °C) and the mass loss was measured for 600 min (10 h).

Thin Film Deposition. A custom-built horizontal cold-wall MOCVD reactor equipped with resistive heating and operating under reduced pressure was used for thin film deposition (see SI 18 in the Supporting Information). The films were grown in the temperature range of 650−850 °C on *p*-type Si(100) substrates at a reactor pressure of 1 mbar. Subsequently, on top of the RE nitride film, a copper capping layer was deposited at a reactor pressure of 0.1 mbar and a susceptor temperature of 300 °C, using **5** as the precursor.[32] Approximately 50 mg of the RE compound and 50 mg of **5** were used for each deposition. The RE precursor was vaporized at 125 °C during deposition, while the Cu precursor was evaporated at 25 °C. Prior to deposition, the substrates were ultrasonically cleaned in acetone, ethanol, and deionized water and subsequently rinsed with deionized water (Millipore Water Purification System) and dried under argon stream. High-purity helium (99.9999%, 50 sccm) was used as the carrier gas, and the flow rate was monitored using a mass flow controller (MKS). When ammonia was used as the reactive gas, a flow rate of 50 sccm NH_3 (99.998%) was maintained.

Thin Film Characterization. Crystallinity and phase composition of the films was investigated by carrying out standard out-of plane X-ray diffraction (XRD) analysis in a Bruker Model AXS D8 Advance diffractometer ($\theta/2\theta$ Bragg−Brentano geometry), using Cu Kα radiation (λ = 1.5418 Å, acceleration voltage = 40 kV, heating current = 30−40 mA). A parabolic Göbel mirror was mounted in the primary beam path (slit width: 0.2 mm). The (111) reflex of copper, which appears at a

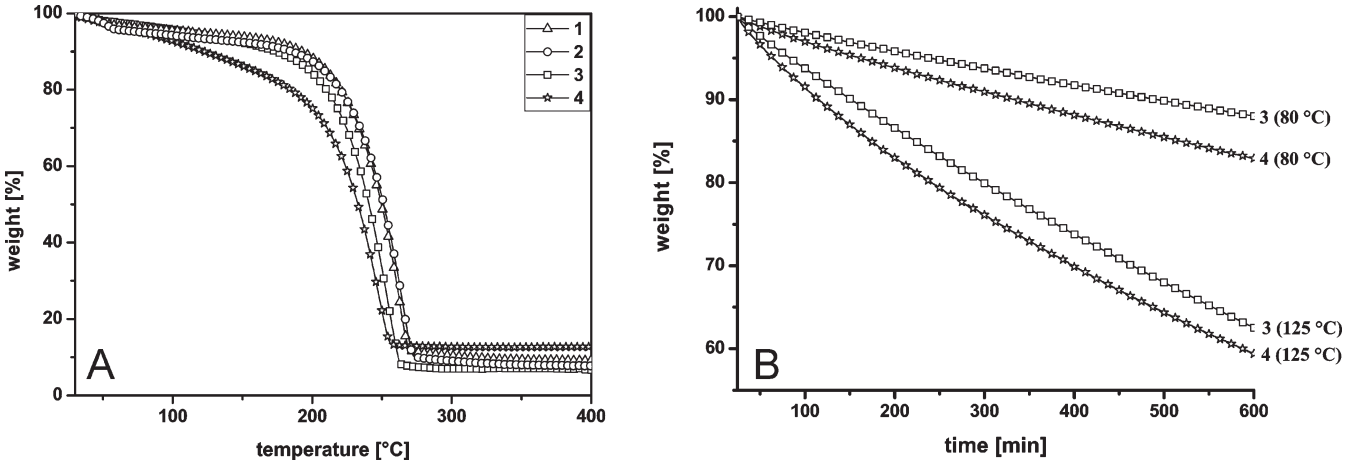

Figure 1. (A) TG curves of **1**−**4**. (B) Isothermal TG curves of **3** and **4** at 80 and 125 °C.

2θ value of 43.298°, was used as an internal standard. XRD data was recorded in a 2θ-angle range of 20°−80° with a step size of 0.014° (1 s per step). Surface morphology was studied with scanning electron microscopy (SEM; LEO; Zeiss). Film composition was determined by nuclear reaction analysis (NRA) and Rutherford backscattering analysis (RBS) at the 4 MV accelerator of the Dynamitron-Tandem-Laboratory at the Ruhr-University of Bochum. The RBS measurements have been performed using a singly charged He beam with energy of 2 MeV and a beam current of 20−40 nA. A silicon surface barrier detector was placed at an angle of 160 degree with respect to the beam axis having a solid angle of 1.911 msrad. For the NRA measurements, element-specific γ-rays induced by a deuteron beam[34] were detected with a high-purity germanium detector operating at 100% relative efficiency. The samples were tilted by 45° toward the detector which had an angle of 90°, with respect to the beam axis. Typical beam currents on the samples were in the range of 40 nA in an area of ~1 mm in diameter, while the collected charge for a sample was ~25 μCoulomb. A polyimide of known chemical composition (Kapton) was used as a standard to obtain the ratios of C, N, and O from the γ-ray yields. X-ray photoelectron spectroscopy was performed in a VersaProbe spectrometer from Physical Electronics, operating with monochromatic Al Kα (1486.6 eV) radiation. The energy position of each spectrum was calibrated with respect to the $4f_{7/2}$ core level of a clean gold sample at 83.8 eV. Broad-range spectra were recorded with a pass energy of 117.4 eV, and the core levels were recorded with a pass energy of 23.5 eV. In situ cleaning of the sample surface and depth profiling of the samples was realized by in situ Ar^+ bombardment at 4 kV (ion current density of 0.54 $\mu A/mm^2$), and 2 kV (ion current density of 0.126 $\mu A/mm^2$) respectively. When necessary, sample charge neutralization was performed by the simultaneous irradiation of the sample surface with low energy electron and Ar ion beams.[35] Integral magnetic measurements were performed using a commercial SQUID magnetometer (Quantum Design MPMS XL5) applying the magnetic field in the film plane. Magnetism/hysteresis ($M(H)$) curves were recorded at 300 and 5 K, respectively. $M(T)$ curves were measured while warming in a field of 10 mT, before the sample was either field-cooled (FC) from 300 K to 5 K in a 4-T field or zero-field-cooled (ZFC) after demagnetizing the sample in an oscillatory field at 300 K. The diamagnetic contribution was derived from the $M(H)$ behavior at high magnetic fields at 300 K and was subtracted from the magnetization data.

RESULTS AND DISCUSSION

Precursor Evaluation. As we presented the thermal properties of the guanidinate compounds **1** and **2** in a previous communication (mentioned in the Introduction[25]), we complement the data set on **1**−**4** by performing thermogravimetric analysis (TGA) as well as isothermal TG measurements for the new amidinate compounds **3** and **4** (see Figures 1A and 1B).

For both amidinato compounds, a slight mass loss is observed, starting at a temperature of 50 °C. Both compounds exhibit a single-step mass loss that sets in at ca. 210 °C. At 260 °C, no further mass loss is observed. The residual masses of both compounds (**3** = 6.8%; **4** = 12.7%) are very much lower than the calculated residual mass for pure GdN or Gd_2O_3 (29.5%, 62.4%) or DyN and Dy_2O_3, respectively (30.1%, 63.6%), indicating that the precursors sublime quite well before they start to decompose. (Also, some hydrolysis may be taken into account, because of trace impurities of the carrier gas and leakage of the TGA instrumentation. In addition, we attribute the slight weight loss at the beginning of the TG measurements to the partial decomposition of the precursors, which is due to short exposure to air during the sample loading procedure.) The dysprosium species seems to be more volatile at low temperatures, whereas the gadolinium compound shows a higher overall mass loss. Comparing the TG curves of the amidinato compounds **3** and **4** to the TG curves of the guanidinato compounds **1** and **2**, it is clearly visible that all four compounds exhibit a single step mass between 200 °C and 270 °C. The values for the residual masses of the guanidinato compounds (**1** = 9.12%, **2** = 7.7%) are comparable to those of the amidinato compounds. Because of the facts that (i) the mass loss of the amidinato compounds between 30 °C and 200 °C (**3** = 16%, **4** = 25%) is comparable to that of the guanidinato compounds (**1** = 12%, **2** = 13%) and (ii) that the single step mass losses of the amidinato compounds start at temperatures comparable to that of the guanidinato compounds, we conclude that **3** and **4** exhibit a thermal performance comparable to **1** and **2**. Thus, **3** and **4** were selected for evaluation of the mass transport behavior. Isothermal TG studies at a temperature of 80 and 125 °C and atmospheric pressure under N_2 were performed. The results are displayed in Figure 1B. (For comparison, isothermal TG studies of the guanidinato compounds **1** and **2** can be found in SI 1 in the Supporting Information). At each temperature, a weight loss with an almost-constant rate over a time period as long as 10 h was observed, and total mass losses within 10 h of 12% (80 °C) and 38% (125 °C) for **3** and 18% (80 °C) and 41% (125 °C) for **4** were obtained, indicating that compound **4** is slightly more

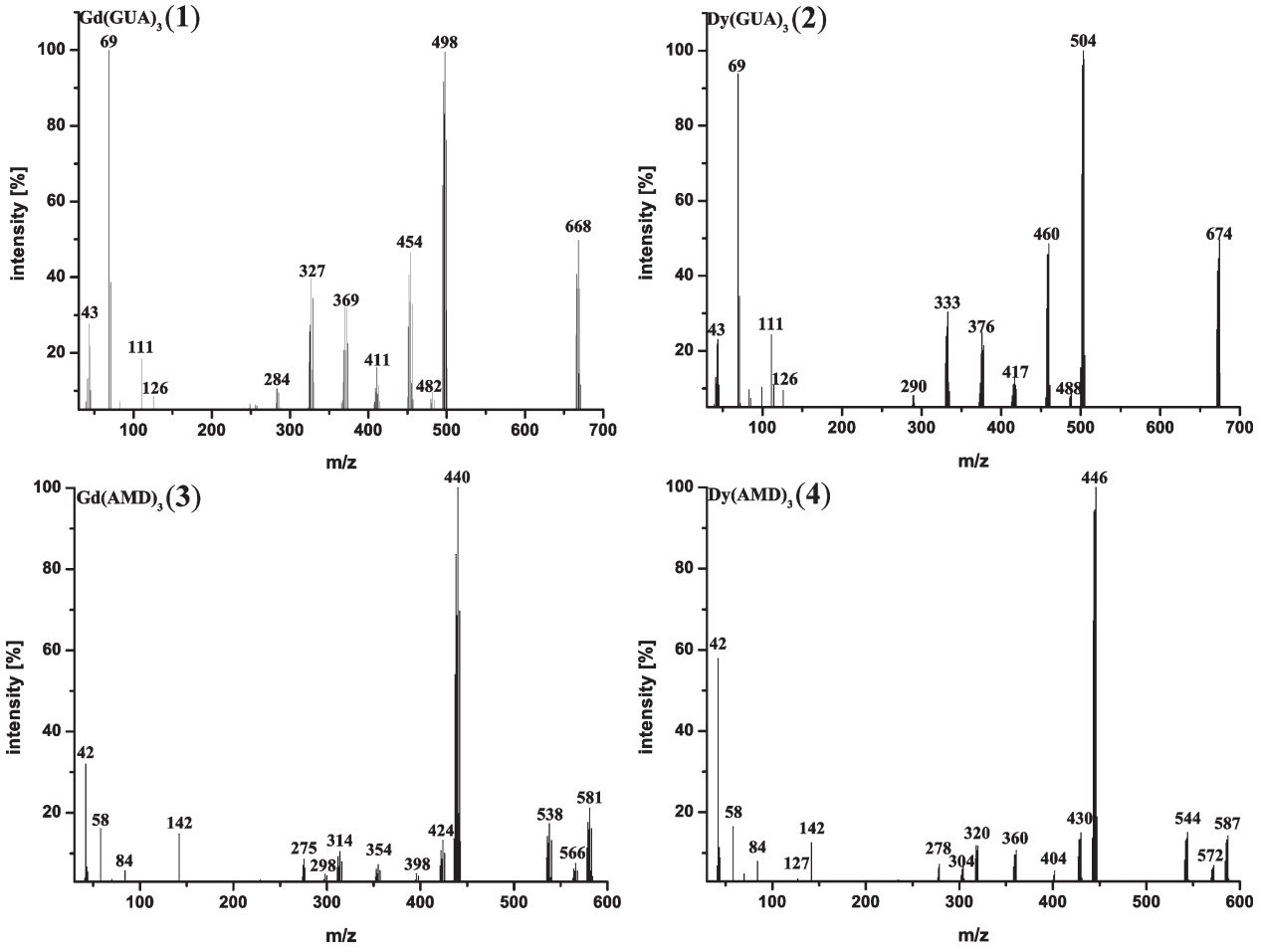

Figure 2. EI-MS data of compounds **1**−**4**. For the sake of clarity, all mass envelopes with an intensity below 5% (for **1** and **2**) and 3% (for **3** and **4**) have been omitted in the presented spectra.

volatile than compound **3**. The slight curvature in the TG curves might be due to the accumulation of nonvolatile material at the surface of the solid precursor. Nevertheless, another explanation for the slight curvature might be a sintering process of the crystallites of the solid precursor during the heating process, which leads to a decrease in surface area and, as a result, a decrease in the amount of subliming material (sublimation rate). This result matches the results of the TG analysis discussed above. The results of the isothermal TG studies clearly show that compounds **3** and **4** are thermally stable at the given temperatures, thus being likely to provide a stable mass transport over a considerable time.

EI-MS Studies. EI-MS analysis of **1** and **2**, shown in Figure 2, revealed that the EI-fragmentation patterns of both compounds are quite similar, indicating a similar decomposition mechanism under EI-MS conditions. Furthermore, two signals at m/z = 668 and m/z = 674, which can be attributed to the molecular ions (M^+) of **1** and **2**, are clearly visible in the EI-MS spectra, indicating that both compounds can be sublimed without decomposition. A complete list of the observed signals in the EI-MS spectra of **1** and **2** is given in SI 2 and SI 3 in the Supporting Information. Furthermore, the fragmentation of the guanidinato compounds **1** and **2**, under EI conditions, was characterized by high-resolution mass spectroscopy, and a general mechanism was proposed for this type of precursor.[11,25,36] The most important finding is the appearance of RE imido species, such as $[\{(^i\mathrm{PrN})_2\mathrm{CNCH}_2\}\mathrm{RENH}]^{+\bullet}$ [RE = Gd (**1**); Dy (**2**)], during fragmentation. To prove the existence of these RE imido species, HR EI-MS analyses of selected mass envelopes observed in the low-resolution EI-MS were conducted. The mass envelope that belongs to the RE imido fragments $[\{(^i\mathrm{PrN})_2\mathrm{CNCH}_2\}\mathrm{RENH}]^{+\bullet}$ with the chemical formula $C_8H_{17}N_4RE$ was chosen for the high-resolution EI-MS experiments. The very small deviation between the calculated and observed masses (Δm = −15.7 mDa for **1** and Δm = −13.8 mDa for **2**) strongly supports the assignments of the observed peaks to the fragments $[\{(^i\mathrm{PrN})_2\mathrm{CNCH}_2\}\mathrm{RENH}]^{+\bullet}$ in both cases **1** and **2**. Although the conditions of EI-induced fragmentation in high vacuum and the thermally activated fragmentation under CVD conditions at reduced pressure cannot be directly compared, the existence of RE imido fragments during EI-MS fragmentation could be an indication that these complexes might contribute to the formation of RE nitride material under single-source-precursor MOCVD conditions, which was confirmed for compound **1**.[11] Similar investigations were carried out with the amidinates **3** and **4**. As expected from **1** and **2**, the EI-fragmentation patterns of compounds **3** and **4** are very similar and the relative intensities of the discrete mass envelopes are almost identical (see Figure 2). The origin of all visible mass envelopes can be nicely explained. The mass envelopes that correspond to the molecular ion peaks (M^+) of **3** (m/z = 581; 21% relative intensity) and **4** (m/z = 587; 14% relative intensity) are clearly seen. The first fragmentation

dx.doi.org/10.1021/cm102840v |*Chem. Mater.* 2011, 23, 1430–1440

step can be attributed to the abstraction of one methyl group from the molecular ion ($M^{+\bullet}$-15), leading to a mass envelope at m/z = 566 for compound **3** and m/z = 572 for compound **4**. The following mass envelope at m/z = 538 for **3** and at m/z = 544 for **4** is assigned to the cleavage of an isopropyl group from the molecular ion ($M^{+\bullet}$-43). The dominant mass envelopes (relative intensity = 100%) in both spectra (**3**: m/z = 440; **4**: m/z = 446) belong to a fragment that is created by the abstraction of one complete amidinato ligand from the molecular ion ($M^{+\bullet}$-141). All further observed mass envelopes can be assigned to distinctive fragmentation products of the molecular ions of **3** and **4**. A list of the detected mass envelopes can be found in SI 4 and SI 5 in the Supporting Information.

Special attention is given to the mass envelopes at m/z = 314 for compound **3** and at m/z = 320 for compound **4**. From the low-resolution EI-MS data, a distinction between two possible fragments for these two mass envelopes is not possible; namely, one consists of a RE atom coordinated by one amidinato ligand and one methyl group $[\{(^i\mathrm{PrN})_2\mathrm{CMe}\}\mathrm{RECH_3}]^{+\bullet}$ (**A**) and another species contains a RE atom coordinated by one amidinato ligand and one imido group $[\{(^i\mathrm{PrN})_2\mathrm{CMe}\}\mathrm{RENH}]^{+\bullet}$ (**B**). To distinguish between these two species, we employed HR EI-MS. Furthermore, we used HR EI-MS to confirm the assignment of the molecular ions $[\mathrm{RE}\{(^i\mathrm{PrN})_2\mathrm{CMe}\}_3]^{+\bullet}$ (**C**). The data of the HR EI-MS analyses are listed in SI 6 in the Supporting Information. With a deviation of 4.5 mDa for **3** and 0.2 mDa for **4** between the calculated and measured masses for the molecular ions of **3** and **4**, the presence of the molecular ion can be verified unambiguously, indicating that compounds **3** and **4** can be sublimed without decomposition, which matches the revelation from thermal analysis. Most interestingly, the HR EI-MS data reveal that the mass envelopes at m/z = 314 and m/z = 320 can be attributed to RE-alkyl species, where a methyl group is bound to the RE metal atom, again substantiated by the insignificant deviation of the observed masses from the calculated masses for fragment **A**. Obviously, the fragmentation pattern of **3** and **4** differs clearly from the results of the HR EI-MS analyses of compound **1** and **2**, where the presence of RE imido fragments was confirmed. This comparison suggests a different behavior of the guanidinates and amidinates under MOCVD conditions. It seems that **3** and **4** should be less suitable as single-source precursors (SSPs) for the rare-earth nitrides (RENs) than **1** and **2**.

MOCVD Experimental Conditions and Growth Rates. Compounds **1**−**4** were evaluated as precursors for REN thin film deposition, using a custom-built thermal MOCVD reactor. In a first set of experiments the depositions were carried out in the absence of additional nitrogen sources (e.g., NH_3, N_2), denoted as single source precursor (SSP) conditions. In a second series of experiments, the influence of ammonia as a reactive gas and potential additional nitrogen source was tested in the same MOCVD apparatus. The applied deposition parameters are listed in the Experimental Section. In each case, uniform films were obtained on standard *p*-type Si(100) substrates in the temperature range of 650−850 °C and the films were coated by a protective layer of copper in a subsequent MOCVD step, as described in the Experimental Section. The film growth rates (given in units of nm/min) were derived from the physical REN layer thicknesses, determined from the cross-sectional SEM measurements, revealing lower growth rates of **1** and **2**, when compared to **3** and **4**. Whereas precursors **1** and **2** show maximum growth rates of ∼8 nm/min at 850 °C when used under SSP conditions and ∼16 nm/min when used in the presence of ammonia, precursors **3** and **4** show maximum growth rates of ∼25 nm/min at 850 °C when used under SSP conditions and ∼31 nm/min when used in the presence of ammonia. This result might be due to a higher sublimation rate of **3** and **4**, compared to that of **1** and **2**. Another explanation for the observed variations in the growth rates for the amidinato and guanidinato compounds can be a difference in the density of the grown films. Nevertheless, a detailed investigation of this aspect is quite technical and beyond the scope of this publication.

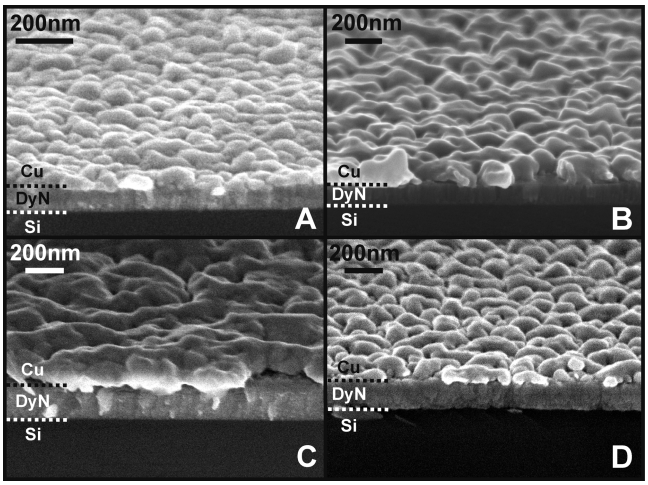

Figure 3. SEM cross-sectional images of (A) a DyN film deposited at 850 °C using **2** under SSP conditions, (B) a DyN film deposited at 650 °C using **2** as a precursor and ammonia as a reactive gas, (C) a DyN film deposited at 850 °C using **4** under SSP conditions, and (D) a DyN film deposited at 850 °C using **4** as a precursor and ammonia as a reactive gas.

Scanning Electron Microscopy (SEM) Imaging and Morphology. All the obtained coatings of a typical thickness of 200 nm were smooth and densely grown with a distinct interface to the protective copper layer. SEM images of DyN films deposited under SSP conditions and in the presence of ammonia, using **2** and **4**, as precursors are shown in Figures 3A−D. (SEM images of GdN films deposited under SSP conditions and in the presence of ammonia using **1** and **3** as precursors can be found in SI 7 in the Supporting Information.)

The SEM images of typical DyN films deposited at 850 °C using **2** and **4** under SSP conditions are shown in Figures 3A and 3C; these serve as representative examples for the entire series of SSP experiments. The copper layer ∼150 nm thick appears to be rough and seems to consist of individual copper crystallites that are sintered together, indicating some island growth mechanism. Cu MOCVD on metal nitride surfaces (e.g., on TiN or TaN surfaces) is known to suffer from nucleation inhibition, leading to island growth and rough coatings.[37,38] The morphology of films grown in the presence of ammonia turned out to be quite similar to the respective SSP grown films. Figures 3B and 3D display representative examples of typical DyN films deposited using **2** and **4** as precursors in the presence of ammonia as a reactive gas. Again, the deposited copper layer seems to consist of larger, coalescent crystallites, as discussed for the SSP case. Note the interface between the silicon substrate and the DyN film, as well as the interface between the DyN film and the copper layer.

X-ray Diffraction (XRD) Studies, Crystallinity, and Phase Composition. The films were characterized by X-ray diffraction (XRD) immediately after deposition, to minimize oxidation.

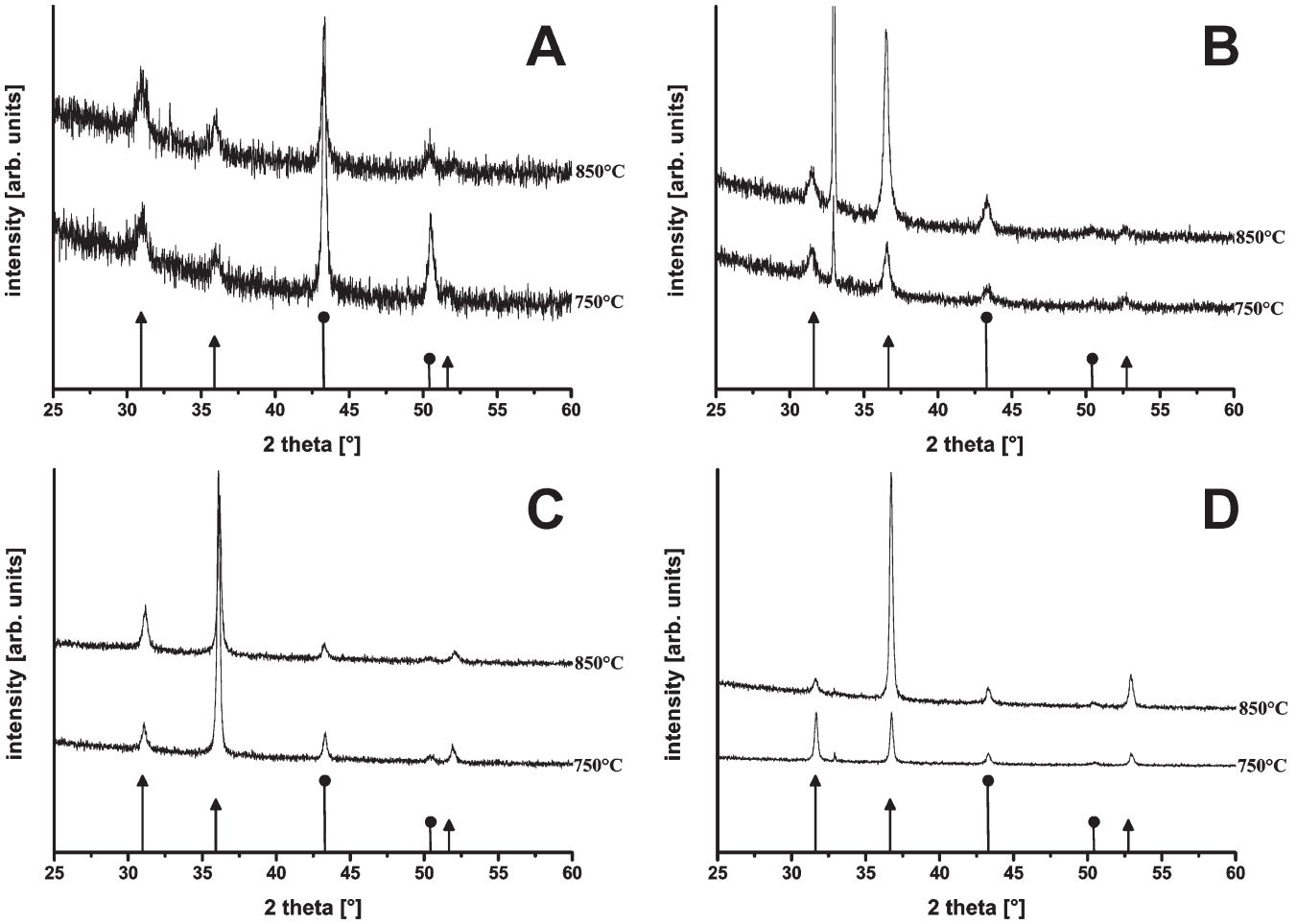

Figure 4. X-ray diffraction (XRD) patterns of REN films grown on Si(100) at 750−850 °C using (A) **1** and (B) **2** as single-source precursors (SSPs) and (C) **3** and (D) **4** as precursors in the presence of ammonia. (In panels A and C, the solid triangle symbol (▲) denotes a peak indexed according to JCPDS Powder Diffraction Card No. 00-015-0888 (GdN); in panels B and D, the same symbol denotes a peak indexed according to JCPDS Powder Diffraction Card No. 00-015-0884 (DyN). The solid circle in all panels denotes peaks assigned from copper (Powder Diffraction Card No. 00-004-0836). The sharp reflex at ∼33° arises from the substrate.)

Using the guanidinato complexes **1** and **2** under SSP conditions at 750 and 850 °C, rock-salt GdN and DyN are deposited, as can be easily deduced from the XRD patterns (see Figures 4A and 4B). The two reflexes at 2θ values of 30°−40° are indexed as the (111) and (200) reflexes of fcc-GdN and fcc-DyN (triangles). The Cu capping layers leads to reflections at 43.29° (111) and 50.43° (200) (denoted by the solid circle symbol). No other crystalline phases (e.g., oxides) were detected. Films deposited at 650 °C show significantly less intense and broader reflexes in addition to the sharp copper reflexes, indicating that the crystallite domain size is much smaller and the REN films tend to become amorphous. In the case of DyN, the intensity of the (200) reflex increases with increasing deposition temperature, indicating preferentially oriented DyN crystallites at high deposition temperatures. However, the amidinato compounds **3** and **4** lead to amorphous films when used under SSP conditions, irrespective of the deposition temperature. Only the reflections for fcc-Cu are seen (see SI 10 and SI 11 in the Supporting Information).

In summary, the compounds **1** and **2**, vs **3** and **4**, behave quite differently when used to deposit the respective REN films. Obviously, our conclusion, which is drawn from the EI-MS studies, that fragmentation of the amidinate ligands in the absence of additional ammonia is not favorable for deposition of crystalline REN films, is substantiated. (Also see SI 8−15 in the Supporting Information for full documentation of all of the XRD data on REN thin film MOCVD using **1**−**4**.)

The lattice parameters of the GdN and DyN films presented in Figures 4A−D were calculated from the positions of the respective (200) reflections. A table containing all calculated lattice parameters can be found in SI 16 in the Supporting Information. The obtained values for the lattice parameters of the deposited GdN films range from 4.981 ± 0.005 Å to 4.999 ± 0.005 Å, which concurs well with the known lattice parameter of unstrained fcc-GdN (4.999 ± 0.005 Å).[39] Furthermore, the obtained lattice parameters are comparable to the data on GdN thin films reported by Gerlach et al. for GdN thin films grown via ion-assisted deposition (IAD), capped with a GaN protecting layer (a = 4.97 ± 0.06 Å).[9] The values obtained for the lattice parameters of the deposited DyN films range from 4.893 ± 0.005 Å to 4.916 ± 0.005 Å, which is comparable to the literature reported value of the lattice parameter for unstrained fcc-DyN (4.905 ± 0.005 Å).[40] Lattice parameters of DyN synthesized by solid-state chemistry methods were found to be in the range of 4.83 Å[41,42] to 4.91 ± 0.01 Å,[43] which match quite well with our results. A comparison of the obtained lattice

dx.doi.org/10.1021/cm102840v |*Chem. Mater.* 2011, 23, 1430–1440

Table 1. Ratios of the Elements of the REN Films Obtained from RBS and NRA Analysis

	SSP				With Ammonia			
	1	2	3	4	1	2	3	4
RBS RE/N	1.0	1.1	2.8	3.2	1.3	0.7	1.2	1.1
RBS RE/C	2.0	3.5	0.3	0.8	6.1	2.5	n.d.	n.d.
RBS RE/O	12.5	0.5	1.8	1.6	2.3	1.5	2.8	1.8
NRA C/N	0.34 ± 0.22	0.31 ± 0.46	8.9 ± 1.0	4.7 ± 1.6	0.22 ± 0.16	0.37 ± 0.05	≤0.2	≤0.3
NRA O/N	0.047 ± 0.13	2.1 ± 0.2	1.6 ± 0.2	2.6 ± 0.7	0.58 ± 0.06	0.60 ± 0.04	0.41 ± 0.08	0.60 ± 0.12

parameters with other known phases such as Gd_xC_y, Dy_xC_y, Gd_xO_y, Dy_xO_y, and $Gd_xC_yO_z$ did not lead to any consistency. (See SI 17 in the Supporting Information.) Furthermore, it was reported that the lattice parameter of GdN and DyN is dependent on the amount of oxygen incorporated in the material to form a solid solution. It was found that, for a material of the composition $Gd_{1.00}N_{0.88}O_{0.12}$, the lattice parameter decreases to a value of 4.96 ± 0.01 Å,[44] and for a material of the composition $Dy_{1.00}N_{0.88}O_{0.12}$, the lattice parameter is reduced to 4.892 ± 0.005 Å.[45] Comparing these results to the lattice parameters presented in SI 16 in the Supporting Information, we can assume that the amount of oxygen incorporation in the as-deposited REN films is low, with ∼10 at. % as the upper threshold.

Chemical Composition and Film Purity. Nuclear reaction analysis (NRA) and Rutherford backscattering analysis (RBS) were performed to quantify the atomic ratio of the light elements C/N and O/N (NRA) and the ratio between the light elements and Gd and Dy (i.e., RE/N, RE/C, and RE/O) (RBS) throughout the volume of the films. The data are compiled in Table 1. Note, that RBS also revealed the presence of copper. Obviously, copper diffused along the REN grain boundaries into the bulk of the films during MOCVD of the Cu capping layer, despite the existence of a macroscopic interface between the copper layer and the underlying REN film, as seen by SEM. We start our discussion with the NRA and RBS analysis of the films deposited under SSP conditions at 850 °C (left columns of Table 1). High O/N values of up to 2.6 : 1 were found by NRA. As deduced from the XRD data above, substantial incorporation of oxygen during deposition is unlikely. Rather, the high O/N ratio by NRA might be explained by insufficient protection of the as-deposited REN films by the Cu layer. Oxygen diffusion may take place along grain boundaries when the films are stored and handled in air for some time, because this was the case when the films were prepared for the NRA and also for the RBS and XPS measurements discussed below. Nevertheless, the copper layer at least slows the oxidation process of the REN thin films and prevents complete oxidation. Most interestingly, the C/N values obtained by NRA for the films deposited with **1** and **2** as SSPs is comparably low (up to ∼0.3), whereas the corresponding C/N value of the films deposited with **3** and **4** as SSPs is very high (up to ∼9). This result matches with the characteristically different XRD data of the films discussed above. The films deposited with the guanidinato complexes as SSPs clearly contain GdN and DyN phases contaminated with some C and O impurities, whereas the films deposited with the amidinato compounds as SSP are amorphous and are heavily contaminated with carbon. The RBS data of these films confirm the NRA results. The measurements revealed RE/N ratios of 1.0 (**1**) and 1.1 (**2**), as expected for fcc-GdN and fcc-DyN. The RE/C (RE/O) ratios were determined to be 2.0 (12.5) for **1** and 3.5 (0.5) for **2**. The

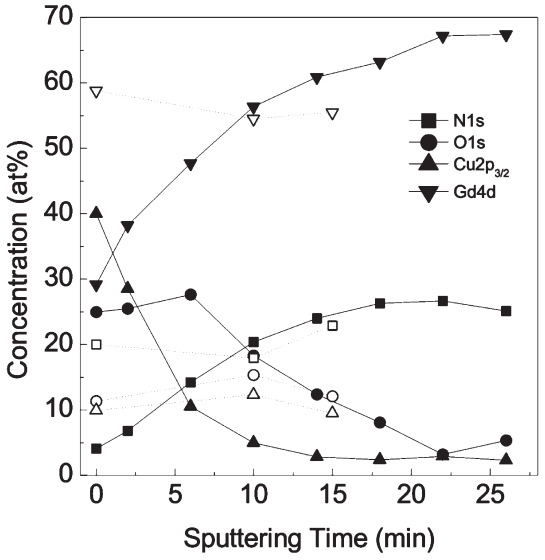

Figure 5. XPS depth profile derived from the survey spectra of **S1** (where **1** was used as the SSP; denoted by open symbols) and **S3** (where **3** was used with NH_3; full symbols) after subsequent Ar ion sputtering (2 kV). The time = 0 reference corresponds to the situation of the samples after 2 min of sputtering at an energy of 4 kV.

RBS data of the films grown with the amidinates **3** and **4** as SSPs reveal RE/N ratios of 2.8 (**3**) and 3.2 (**4**). The RE/C (RE/O) ratios were 0.3 (1.8) for **3** and 0.8 (1.6) for **4**. Thus, the NRA and RBS data clearly show a much less-efficient nitrogen incorporation into the films grown from amidinates as SSPs, as expected from the HR EI-MS studies. The right-hand columns of Table 1 show the drastic effect of additional ammonia as a reactive gas on the C, N, O elemental composition of the obtained films. The oxygen contamination is somewhat lower (O/N up to 0.6) than that for SSP conditions. Interestingly, the C/N value of ∼0.3 is almost unchanged in case of the guanidinates **1** and **2**. In contrast, films grown from the amidinates **3** and **4** reveal significantly reduced C/N values of ∼0.3. The corresponding RBS analyses of the films confirm the NRA results. The RE/N (RE/O) [RE/C] ratios were 1.3 (2.3) [6.1] for **1** and 0.7 (1.5) [2.5] for **2**. The corresponding RE/N (RE/O) values for the amidinate precursors were 1.2 (2.8) for **3** and 1.1 (1.8) for **4**. Carbon impurities were not detected in the case of **3** and **4**. RBS and NRA results indicate that the guanidinato compounds **1** and **2** efficiently produce REN thin films under SSP conditions, whereas the amidinato compounds **3** and **4** are capable of producing high-purity REN films only when ammonia is used as the reactive gas.

The elemental composition was further analyzed by XPS and Ar-ion sputtering, to obtain depth profile information. For this

dx.doi.org/10.1021/cm102840v |*Chem. Mater.* 2011, 23, 1430–1440

Table 2. Ratios of the Elements Inside the Rare-Earth Nitride (REN) Films Obtained from X-ray Photoelectron Spectroscopy (XPS) Analysis

	1 Used as SSP (Sample **S1**)			**3** Used with NH_3 (Sample **S3**)						
sputtering time at 2 kV (min)	0	10	15	0	6	10	14	18	22	26
XPS RE/N (±1 at. %)	3	3	2	7	3	3	3	3	3	3
XPS RE/O (±1 at. %)	5	4	5	1	2	3	5	8	21	13

purpose, two GdN thin film samples were chosen, for which the previous analyses revealed that they consist of the best-quality GdN that we could get with our methods. Both samples were grown at 850 °C, either using **1** as SSP (**S1**) or **3** together with ammonia (**S3**) (see Figure 5).

XPS analysis of both films as-deposited showed high levels of copper, carbon, and oxygen at the surface (data not shown). However, no traces of gadolinium or nitrogen could be detected, indicating that there was no diffusion of gadolinium or nitrogen to the surface during the deposition of the copper layer. The samples were then sputtered for 2 min with Ar ions of 4 kV energy, until the signals corresponding to Gd and N were clearly visible. After this first sputtering step, the samples were further sputtered at a lower rate with 2 kV energy ions. The stoichiometry (from survey spectra) corresponding to each step for the 2 kV sputtering case can be seen in Figure 5.

Sample **S1** (where **1** was used as an SSP; see open symbols in Figure 5) was sputtered for up to 20 min with 2 kV of energy, at which point the silicon substrate was reached. This sample showed a constant concentration of copper (~10 at. %) along the GdO_xN_y film. The carbon content could not be determined exactly by XPS, because of an overlap of the C 1s peak with the Gd 4p doublet. Nevertheless, it could be estimated that the carbon level inside the film was <2 at. %. The RE/O and RE/N ratios did not vary much along the film. However, they were higher than the values obtained from RBS or NRA (see Table 2). This result may be explained by preferential sputtering of oxygen and nitrogen atoms.

Sample **S3** (where **3** was used with NH_3; see solid symbols in Figure 5) was sputtered for up to 26 min with 2 kV of energy. In this sample, it was possible to see a clear decrease in copper concentration, which reached a steady value of ~2 at. % after 15 min of sputtering. This may be due to better crystallinity or higher density of this film, compared to **S1**. However, the signals corresponding to the Gd 4d doublet and the O 1s peak did not reach a steady state. This does not necessarily indicate a real concentration gradient within the film, but it could be due to the preferential sputtering of oxygen (see Table 2).[46] As in the previous sample, no clear C 1s signal was observed.

In Figure 6, we can see the XPS spectra corresponding to the core levels of Gd 4d, O 1s, and N 1s of **S1**, after 2 min of sputtering with Ar ions at 4 kV plus 10 min of sputtering with Ar ions at 2 kV. The Gd 4d peak shows multiplet splitting, because of interaction of the 4d photohole with the $4f_7$ valence band electrons, forming ^9D and ^7D final ionic states.[47] The ^9D component was fitted using the relative ^9D peak positions and intensities of pure metal, with pure Gaussian lines of width 2.5 eV. According to the literature,[48] the relative intensities (positions) of the ^9D peaks ($\overline{J}$ = 5, 4, 3, 2), with respect to the main $\overline{J}$ = 6 peak, are 0.88 (+1.02 eV), 0.7 (+2.01 eV), 0.52 (+3.0 eV), and 0.34 (+3.92 eV). The ^7D components were approximated by a single Gaussian of width 4.0 eV. The background in this case was fitted using a Shirley function modified by a second-grade polynomial.

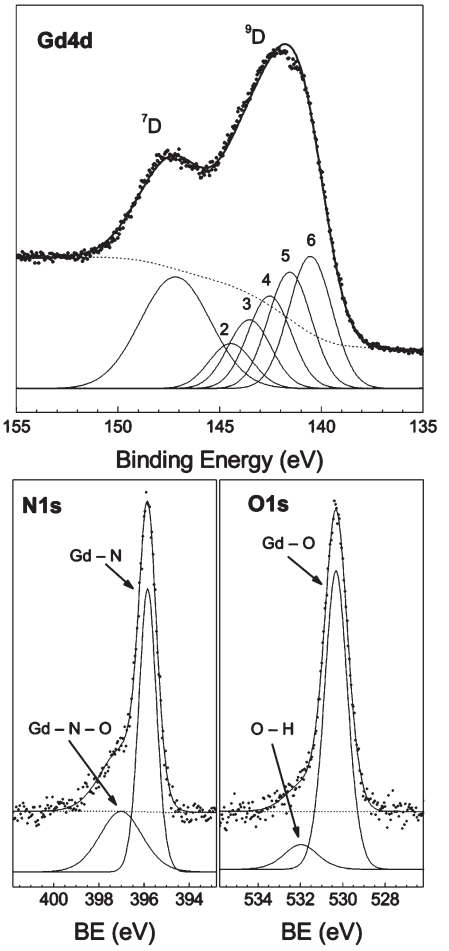

Figure 6. XPS core levels of Gd 4d, N 1s, and O 1s of the GdN sample deposited at 850 °C using **1** as an SSP (sample **S1**).

We found the binding energy (BE) position of the $\overline{J}$ = 6 component to be 140.5 eV. In the case of pure metal, the Gd 4d BE position is reported in the literature to be between 140.4 eV[48,49] and 141.6 eV.[50] For Gd_2O_3, the values reported oscillate between ~141.8 eV[48] and 143.5 eV.[50,51] The profile that we measured shows a profile similar to those reported in the literature for Gd_2O_3.[48,50] However, in the present case, the lines are broader (a full width at half maximum (fwhm) of 2.5 eV is observed for the ^9D lines) than, for example, those reported by Gupta et al. (who used a pure Gd_2O_3 sample with an fwhm value of 2.2 eV).[48] This fact, and the fact that we see the peak maximum at a relatively low BE position, could be compatible with the presence of a mixture of metal, nitride, and oxide phases with BE positions in the range between 140.5 eV (rare-earth metal and/or REN) and 142−143.5 eV (oxide). Unfortunately, we have not found any reference with regard to the expected BE position of GdN compounds. However, the presence of metallic Gd is

dx.doi.org/10.1021/cm102840v |*Chem. Mater.* 2011, 23, 1430–1440

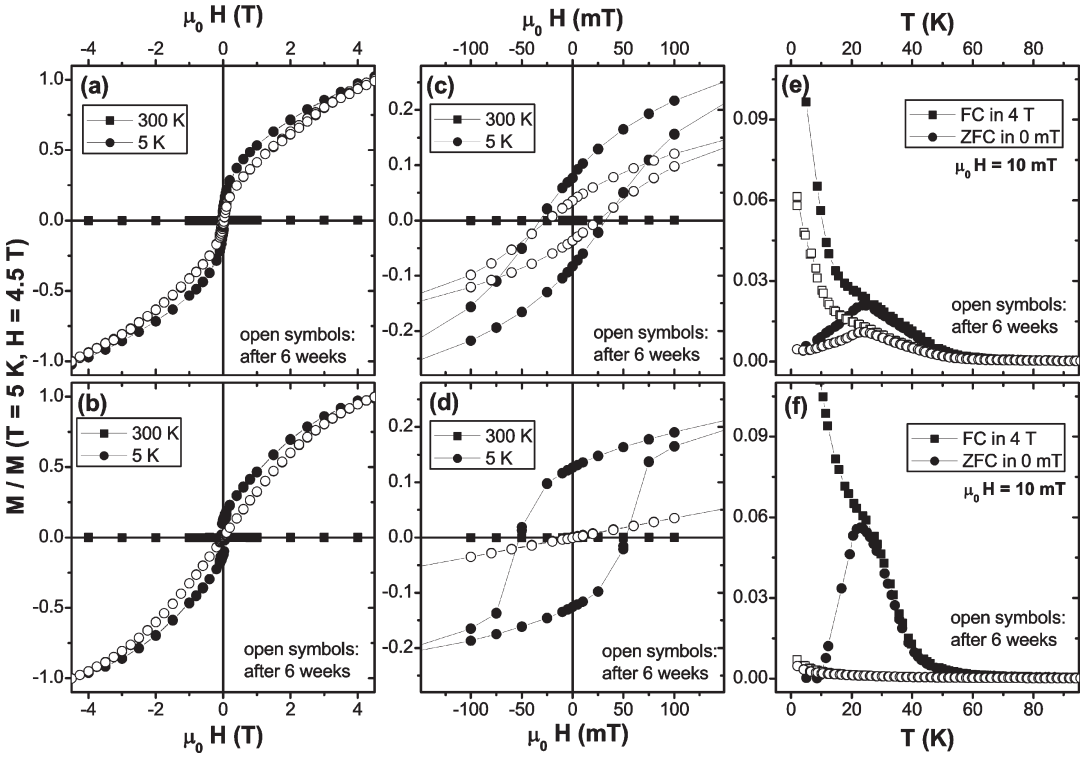

Figure 7. Upper row: $M(H)$ and $M(T)$ curves of a GdN film grown at 850 °C, using **1** as an SSP (sample **S1**); lower row: $M(H)$ and $M(T)$ curves of a GdN film grown at 850 °C using **3** as a precursor in the presence of ammonia (sample **S3**).

unlikely, because it was not detected by other techniques, such as XRD. On the other hand, the analysis of the N 1s and O 1s lines support the interpretation that the deposited film consists of a mixture of nitride and oxide phases or solid solutions GdN_xO_y ($x + y = 1$). The N 1s line shows two components: a main one at a BE of 396.0 eV, and a weaker one at 397.2 eV. We assigned the component at 396 eV to GdN, by comparison with typical N 1s positions of metallic nitrides, which can be expected in the energy range of ~396−398 eV. The second, weaker component could indicate the presence of oxygen-related bonds within the film, such as N−O or Gd−N−O bonds.[48,52] The O 1s line shows a main component at 530.5 eV that we attribute to Gd_2O_3[48] and/or Gd−N−O bonds. There is also a small component at higher BE (532.0 eV) that can be attributed to O−H bonds.[53,55]

Magnetic Measurements. After it was found that the guanidinato compounds **1** and **2** are capable of yielding RE nitride material under single-source conditions and the amidinato compounds **3** and **4** are capable of yielding REN material when they are used as precursors in the presence of ammonia, we were interested in the magnetic properties of the obtained REN materials. SQUID measurements on these two films were conducted. Figure 7 summarizes the magnetic properties of two GdN films grown at 850 °C, either using **1** under SSP conditions (sample **S1**, upper row of Figure 7 (panels a, c, e)) or **3** in the presence of ammonia (sample **S3**, lower row of Figure 7 (panels b, d, f)). In the as-grown state (solid symbols), the samples were transferred under inert atmosphere directly into the SQUID equipment (i.e., under a helium atmosphere, to minimize exposure to ambient conditions to <20 s). The identical measurement protocol was repeated after 6 weeks of exposure to ambient conditions (open symbols).

The $M(H)$ curves at 300 K (denoted as squares in Figure 7) are, in all cases, anhysteretic. At 5 K (data denoted by circles in Figure 7), the $M(H)$ curves are composed of a strong paramagnetic contribution plus a hysteretic contribution, which is clearly visible in the low-field regime (middle panels in Figure 7). This hysteretic contribution is characteristic of either ferromagnetism or blocked superparamagnetism. In the case of sample **S1**, the hysteresis is reduced after 6 weeks, whereas it has completely vanished for sample **S3,** which behaves purely paramagnetic, after 6 weeks. Note that the curvature of the $M(H)$ curve is lower than expected for Gd ions with $S = {}^7/_2$ (not shown). Paramagnetism for **S3** after 6 weeks is further corroborated by the $M(T)$ measurements (right panels in Figure 7). No obvious separation between FC (squares) and ZFC (circles) curves is visible. In contrast, in the as-prepared state, both samples exhibit a clear separation of the FC and ZFC curves below 25 K (sample **S1**) and 20 K (sample **S3**), respectively, which is indicative of hysteretic behavior. This is superimposed by a strong paramagnetic contribution, visible as a $1/T$ contribution at low temperatures. Above 50 K, significant magnetization is no longer detected in either sample.

The magnetic properties as described above are indicative of superparamagnetism of small ferromagnetic grains of GdN ($T_C \approx 60$ K).[55] The absence of any magnetization above 50 K excludes the presence of a significant amount of metallic gadolinium ($T_C = 291$ K). The clear blocking behavior seen in the FC/ZFC experiments points toward small grains of GdN with a broader size and/or magnetic anisotropy distribution for **S1**, as indicated by the broader ZFC maximum. After 6 weeks, the GdN film is partially (**S1**) or fully (**S3**) oxidized as indicated by the increased paramagnetic contribution and the reduced or even absent hysteretic contribution. The material formed by oxidation

dx.doi.org/10.1021/cm102840v |*Chem. Mater.* 2011, 23, 1430–1440

is presumably antiferromagnetic Gd_2O_3 ($T_N \approx 2$ K), which behaves paramagnetic at 5 K. Furthermore, it is known that Gd_2O_3 nanoparticles exhibit similar $M(H)$ behavior at 5 K, as observed for sample **S3** after 6 weeks. Obviously, the smaller grain size of **S3** leads to a faster oxidation of the GdN film.

SUMMARY

The guanidinato complexes **1** and **2** are useful as single-source precursors (SSPs) for metal−organic chemical vapor deposition (MOCVD) of crystalline GdN and DyN materials. Thin films deposited at 850 °C were only slightly contaminated with carbon impurities. The application of ammonia as a reactive gas did not lead to a significant improvement of the purity and crystallinity. In contrast, the amidinato complexes **3** and **4** cannot be used as SSPs for MOCVD of the metal nitrides. The obtained films were amorphous, even at a deposition temperature of 850 °C, and show very high amounts of carbon impurities. This preferred incorporation of carbon over nitrogen, in the case of the amidinate ligands, is in good agreement with the EI-MS data, revealing molecular RE-C species in the course of the fragmentation of the precursors. However, the incorporation of carbon was drastically reduced for the amidinate precursors when ammonia was applied as a reactive gas and films containing highly crystalline fcc-GdN and fcc-DyN were deposited, even at low substrate temperatures of 650 °C. Nevertheless, all deposited films were contaminated with significant amounts of oxygen most likely introduced by post-deposition oxidation (aging) of the films during manipulation and storage. The protective copper layer could not prevent this. Alternative capping layers must be identified to reduce oxygen impurities and to increase the stability of the films under ambient conditions. SQUID measurements of two representative GdN films revealed that the magnetic properties of the deposited films point to the existence of small ferromagnetic grains of GdN, as reported by Leuenberger et al.[55]

Overall, the results demonstrate the general potential of homoleptic, volatile guanidinato and amidinato complexes of rare-earth metals as precursors for MOCVD of the respective rare-earth metal nitride materials. Further studies are needed to better understand the mechanistic details of the different behavior of the guanidinato and amidinato complexes under MOCVD as well as ALD conditions. In particular, alternative capping techniques (e.g., MOCVD of AlN, GaN etc.) will be investigated to better protect the highly sensitive rare-earth nitride films against oxidation/hydrolysis.

ASSOCIATED CONTENT

Supporting Information. This material is available free of charge via the Internet at http://pubs.acs.org.

AUTHOR INFORMATION

Corresponding Author

*E-mails: roland.fischer@rub.de, anjana.devi@rub.de.

ACKNOWLEDGMENT

Dr. R. Neuser and Mr. M. Born are acknowledged for the SEM measurements. T.B.T. and A.P.M. thank the Ruhr-University Bochum Research School for the financial support. The authors acknowledge the most-valuable support from the Ruhr University Research Department, "Plasmas with Complex Interactions" (http://www.rd.ruhr-uni-bochum.de/plasma/index.html). The authors are grateful to the RD-IFSC at Ruhr-University Bochum for supporting this project.

REFERENCES

(1) Aerts, C. M.; Strange, P.; Horne, M.; Temmerman, W. M.; Szotek, Z.; Svane, A. *Condensed Matter* **2003**, Preprint Archive.

(2) Duan, C.-G.; Sabirianov, R. F.; Mei, W. N.; Dowben, P. A.; Jaswal, S. S.; Tsymball, E. Y. *J. Phys.: Condens. Matter* **2007**, 315220.

(3) Khazen, K.; von Bardeleben, H. J.; Cantin, J. L.; Bittar, A.; Granville, S.; Trodahl, H. J.; Ruck, B. *J. Phys. Rev. B* **2006**, *74*, 245330.

(4) Leuenberger, F.; Parge, A.; Felsch, W.; Fauth, K.; Hessler, M. *Phys. Rev. B* **2005**, *72*, 014427.

(5) Zhou, Y. K.; Kim, M. S.; Teraguchi, N.; Suzuki, A.; Nanishi, Y.; Asahi, H. *Phys. Status Solidi B* **2003**, *240* (2), 440.

(6) LaDuca, R. L.; Wolczanski, P. T. *Inorg. Chem.* **1992**, *31* (8), 1311.

(7) Fitzmaurice, J. C.; Hector, A.; Rowley, A. T.; Parkin, I. P. *Polyhedron* **1994**, *13* (2), 235.

(8) Scarpulla, M. A.; Gallinat, C. S.; Mack, S.; Speck, J. S.; Gossard, A. C. *J. Cryst. Growth* **2009**, *311*, 1239.

(9) Gerlach, J. W.; Menning, J.; Rauschenbach, B. *Appl. Phys. Lett.* **2007**, *90*, 061919.

(10) McKenzie, W. R.; Munroe, P. R.; Budde, F.; Ruck, B. J.; Granville, S.; Trodahl, H. *J. Curr. Appl. Phys.* **2006**, *6*, 407.

(11) Milanov, A. P.; Thiede, T. B.; Devi, A.; Fischer, R. A. *J. Am. Chem. Soc.* **2009**, *131*, 17062.

(12) (c) Jones, A. C.; Hitchman, M. L. In *Chemical Vapor Deposition: Precursors, Processes and Applications*; Jones, A. C., Hitchman, M. L., Eds.; RSC: Cambridge, U.K., 2009; Chapter 1. (a) Leskelä, M.; Ritala, M. *Angew. Chem., Int. Ed.* **2003**, *42*, 5548. (b) Knez, M.; Nielsch, K.; Niinistö, L. *Adv. Mater.* **2007**, *19*, 3425.

(13) Selected references on SSPs:(a) Shin, J.; Waheed, A.; Agapiou, K.; Winkenwerder, W. A.; Kim, H.-W.; Jones, R. A.; Hwang, G. S.; Ekerdt, J. G. *J. Am. Chem. Soc.* **2006**, *128*, 16510. (b) Panneerselvam, A.; Malik, M. A.; Afzaal, M.; O'Brien, P.; Helliwell, M. *J. Am. Chem. Soc.* **2008**, *130*, 2420.

(14) Fischer, R. A.; Parala, H. In *Chemical Vapor Deposition: Precursors, Processes and Applications*; Jones, A. C., Hitchman, M. L., Eds.; RSC: Cambridge, U.K., 2009; Chapter 9.

(15) Fix, R. M.; Gordon, R. G.; Hoffman, D. M. *Chem. Mater.* **1993**, *5*, 614.

(16) McElwee-White, L. *Dalton Trans.* **2006**, 5327.

(17) Potts, S. E.; Carmalt, C. J.; Blackman, C. S.; Leese, T.; Davies, H. O. *Dalton Trans.* **2008**, 5730.

(18) Rische, D.; Baunemann, A.; Winter, M.; Fischer, R. A. *Inorg. Chem.* **2006**, *45* (1), 269.

(19) Becker, J. S.; Suh, S.; Wang, S.; Gordon, R. *Chem. Mater.* **2003**, *15*, 2969.

(20) Rische, D.; Parala, H.; Gemel, E.; Winter, M.; Fischer, R. A. *Chem. Mater.* **2006**, *18*, 6075.

(21) Baunemann, A.; Lemberger, M.; Bauer, A. J.; Parala, H.; Fischer, R. A. *Chem. Vap. Deposition* **2007**, *13* (2−3), 77.

(22) Thiede, T. B.; Parala, H.; Reuter, K.; Passing, G.; Kirchmeyer, S.; Hinz, J.; Lemberger, M.; Bauer, A. J.; Barreca, D.; Gasparotto, A.; Fischer, R. A. *Chem. Vap. Deposition* **2009**, *15*, 334.

(23) Rische, D.; Parala, H.; Baunemann, A.; Thiede, T.; Fischer, R. *Surf. Coat. Technol.* **2007**, *201*, 9125.

(24) Baunemann, A.; Bekermann, D.; Thiede, T. B.; Parala, H.; Winter, M.; Gemel, C.; Fischer, R. A. *Dalton Trans.* **2008**, 3715.

(25) Milanov, A. P.; Fischer, R. A.; Devi, A. *Inorg. Chem.* **2008**, *47*, 11405.

(26) Slifirski, J.; Huchet, G.; Reynes, A.; Marty, A.; Teyssandier, F. *Chem. Mater.* **1995**, *7*, 622.

(27) Bchir, O. J.; Johnston, S. W.; Cuadra, A. C.; Anderson, T. J.; Ortiz, C. G.; Brooks, B. C.; Powell, D. H.; McElwee-White, L. *J. Cryst. Growth* **2003**, *249*, 262.

(28) de Rouffignac, P.; Gordon, R. G. *Chem. Vap. Deposition* **2006**, *12*, 152.
(29) Lim, B. S.; Rahtu, A.; de Rouffignac, P.; Gordon, R. G. *Appl. Phys. Lett.* **2004**, *84*, 3957.
(30) Lim, B. S.; Rahtu, A.; Park, J.-S.; Gordon, R. G. *Inorg. Chem.* **2003**, *42*, 7951.
(31) Kim, K. H.; Farmer, D. B.; Lehn, J.-S. M.; Rao, P. V.; Gordon, R. G. *Appl. Phys. Lett.* **2006**, *89*, 133512.
(32) Goel, S. C.; Kramer, K. S.; Chiang, M. Y.; Buhro, W. E. *Polyhedron* **1990**, *4* (9), 6114113.
(33) Becker, R.; Devi, A.; Weiss, J.; Weckenmann, U.; Winter, M.; Kiener, C.; Becker, H.-W.; Fischer, R. A. *Chem. Vap. Deposition* **2003**, *9* (3), 149.
(34) Elekes, Z.; Kiss, A. Z.; Biron, I.; Calligaro, T.; Salomon, J. *Nucl. Instrum. Methods B* **2000**, *168*, 305.
(35) Larson, P. E.; Kelly, M. A. *J. Vac. Sci. Technol. A* **1998**, *16*, 3483.
(36) Milanov, A. Thesis, Ruhr University, Bochum, Germany, 2010.
(37) Kim, D.-H.; Wentorf, R. H., Jr.; Gill, W. N. *J. Appl. Phys.* **1993**, *74*, 5164.
(38) Nuesca, G. M.; Kelber, J. A. *Thin Solid Films* **1995**, *262*, 224.
(39) The International Centre for Diffraction Data PDF (Powder Diffraction File), JCPDS File Card No. 00-015-0888.
(40) The International Centre for Diffraction Data PDF (Powder Diffraction File), JCPDS File Card No. 00-015-0884.
(41) Ettmayer, P.; Waldhart, J.; Vendl, A.; Banik, G. *Monatsh. Chem.* **1980**, *111*, 945.
(42) Ettmayer, P.; Waldhart, J.; Vendl, A.; Banik, G. *J. Nucl. Mater.* **1980**, *91*, 293.
(43) Fitzmaurice, J. C.; Hector, A.; Rowley, A. T.; Parkin, I. P. *Polyhedron* **1994**, *13* (2), 235.
(44) Gambino, R. J.; Cuomo, J. J. *J. Electrochem. Soc.* **1996**, *113* (4), 401.
(45) Takano, M.; Itoh, A.; Akabori, M.; Ogawa, T. *J. Alloys Compd.* **2001**, *327*, 235.
(46) Wong, H. Y.; Ong, C. W.; Kwok, U. R. W. M.; Wong, K. W.; Wong, S. P.; Cheung, W. Y. *Thin Solid Films* **2000**, *376*, 131.
(47) Lademan, W. J.; See, A. K.; Klebanoff, L. E.; van der Laan, G. *Phys. Rev. B* **1996**, *54* (23), 17191.
(48) Gupta, J. A.; Landheer, D.; Sproule, G. I.; McCaffrey, J. P.; Graham, M. J.; Yang, K.-C.; Lu, Z.-H.; Lennard, W. N. *Appl. Surf. Sci.* **2001**, *173*, 318.
(49) Moulder, J. F.; Stickle, W. F.; Sobol, P. E.; Bomben, K. D. *Handbook of X-ray Photoelectron Spectroscopy*: Physical Electronics: Minnesota, 1995.
(50) Terzieff, P.; Lee, K. *J. Appl. Phys.* **1979**, *50* (5), 3565.
(51) Sarma, D. D.; Rao, C. N. R. *J. Electron Spectrosc. Relat. Phenom.* **1980**, *20*, 25.
(52) Baltrusaitis, J.; Jayaweera, P. M.; Grassian, V. H. *Phys. Chem. Chem. Phys.* **2009**, *11*, 8295.
(53) Vasquez, R. P.; Foote, M. C.; Hunt, B. D. *J. Appl. Phys.* **1989**, *66*, 4867.
(54) Bassim, N.; Cracium, V.; Howard, J.; Singh, R. K. *Appl. Surf. Sci.* **2003**, *205*, 267.
(55) Leuenberger, F.; Parge, A.; Felsch, W.; Baudelet, F.; Giorgetti, C.; Dartyge, E.; Wilhelm, F. *Phys. Rev. B* **2006**, *73*, 214430.